Applied Physics Letters ARTICLE scitation.org/journal/apl

High kinetic inductance NbTiN superconducting transmission line resonators in the very thin film limit

Cite as: Appl. Phys. Lett. **121**, 052602 (2022); doi: 10.1063/5.0100961
Submitted: 27 May 2022 · Accepted: 16 July 2022 ·
Published Online: 5 August 2022

Terence M. Bretz-Sullivan,[1,a)] Rupert M. Lewis,[1] Ana L. Lima-Sharma,[1] David Lidsky,[1] Christopher M. Smyth,[1] C. Thomas Harris,[1,2] Michael Venuti,[3] Serena Eley,[3] and Tzu-Ming Lu[1,2]

AFFILIATIONS

[1]Sandia National Laboratories, Albuquerque, New Mexico 87185, USA
[2]Center for Integrated Nanotechnologies, Sandia National Laboratories, Albuquerque, New Mexico 87123, USA
[3]Department of Physics, Colorado School of Mines, Golden, Colorado 80401, USA

[a)]Author to whom correspondence should be addressed: tmbretz@sandia.gov

ABSTRACT

We examine the DC and radio frequency (RF) response of superconducting transmission line resonators comprised of very thin NbTiN films, <12 nm in thickness, in the high-temperature limit, where the photon energy is less than the thermal energy. The resonant frequencies of these superconducting resonators show a significant nonlinear response as a function of RF input power, which can approach a frequency shift of $\Delta f = -0.15\%$ in a -20 dB span in the thinnest film. The strong nonlinear response allows these very thin film resonators to serve as high kinetic inductance parametric amplifiers.

Superconducting transmission line microwave resonators are integral components in quantum circuits for computing and sensing applications and research on resonators can provide crucial information regarding energy loss mechanisms in superconducting circuits.[1–3] Resonators can serve a variety of purposes, such as for circuit quantum electrodynamics studies, as parametric amplifiers, microwave kinetic inductance detectors, current sensors, and stepped impedance bandpass filters.[4–11] A key element to their physical properties is their nonlinear kinetic inductance which manifests itself as a Kerr-like nonlinearity to an applied current. To the lowest order approximation, the kinetic inductance of a superconducting strip is expressed as $L_k(I) \approx L_k(0)[1 + (\frac{I}{I_*})^2]$, where I is the current through a superconducting strip and I_* is on the order of the critical current.[11] The first term, $L_k(0)$, is simply the kinetic inductance of the Cooper pairs. The second term, $L_k(0)[(\frac{I}{I_*})^2]$, describes the nonlinear response to an applied current. This is essential for a resonator to serve as a parametric amplifier and has also been utilized in superconducting resonators for frequency combs and period-tripling subharmonic generation.[12,13]

Recent work has focused on new methods for growth and characterization of superconducting thin films and the characterization of the quality factors and loss mechanisms of coplanar waveguide resonators comprised of Al, Nb, Re, NbN, TiN, and NbTiN superconducting thin films.[14–29] The studies of the quality factors and loss mechanisms in superconducting resonators were primarily focused on methods to improve the coherence times of superconducting qubits often, but not exclusively, in the low-temperature, single-photon limit. NbTiN superconducting films are advantageous over other material systems, since they are easily deposited by DC sputtering at room temperature onto Si substrates, possess uniform properties across large substrates, and exhibit a high kinetic inductance.[30–33]

The high kinetic inductance allows for high-characteristic impedance ($Z_c \gg 50\,\Omega$) superconducting resonators, ideal for coupling resonator photons to systems with small electric dipole moments such as spins in quantum dots.[32,33] NbTiN superconducting films are interesting in their fundamental superconducting properties, for instance, their deviation from a Bardeen–Cooper–Schrieffer theory in terms of their electromagnetic response of strongly disordered films and for studies of the superconductor–insulator transition.[34–36] Taken together, these attributes make NbTiN a favorable material system for superconducting resonator-based parametric amplifiers. Although other superconducting films, such as granular aluminum films, have a larger kinetic inductance ($\sim 1 - 2\,\frac{\text{nH}}{\text{sq.}}$) as compared with NbTiN films, films of granular aluminum have a lower $T_c \sim 2.25$–2.6 K.[37]

The NbTiN films in this study have the combined advantage of a larger T_c as compared to granular aluminum and a higher kinetic inductance compared to previous reported kinetic inductance values on NbTiN superconducting films.[32,33] Both attributes are essential for high temperature operation of a parametric amplifier where heat dissipation and cooling are not an issue. Finally, the resonators are simple to model and are easy to fabricate as compared to Josephson-junction-based parametric amplifiers, albeit without *in situ* magnetic field tunability.[38–40]

In this paper, we present a study of the resonant frequency response of a set of five quarter-wave ($\lambda/4$) NbTiN superconducting transmission line resonators in the very thin film limit, where the film thickness t is below 12 nm. We focus on the high-temperature limit hf ($\sim$4.8 GHz) $< k_B T$ ($\sim$31 GHz), where h is the Planck constant, f is the microwave frequency, k_B is the Boltzmann constant, and T is the temperature. We find that upon decreasing the thickness to 3.36 nm, the kinetic inductance of the films increases to $\approx 0.4\ \frac{\text{nH}}{\text{sq.}}$. Additionally, we find that in the thinnest film, the resonators exhibit an easily measurable bifurcation of the resonance curve at a moderate radio frequency (RF) input power which we attribute to nonlinearity associated with their high kinetic inductance. The resonators' high kinetic inductance, strong nonlinear RF response, and high temperature operation regime make them ideal candidates for resonator-based parametric amplifiers.

We used DC magnetron sputtering to deposit all the NbTiN films used in this study on blank 4-in. Si wafers with a 1 μm thermal oxide cap and varied the deposition time to achieve the desired film thickness. We sputtered our films using a Kurt J. Lesker Physical Vapor Deposition system, which had a typical base pressure of $\sim 2 \times 10^{-7}$ Torr, from a $Nb_{0.67}Ti_{0.33}$ target. The deposition parameters are as follows: deposition pressure of 6 mTorr, Ar carrier gas with 2.2% N_2, and DC deposition power of 100 W. In Fig. 1(a), we display the NbTiN film thickness, as measured by x-ray reflectometry, vs deposition time. See the supplementary material for x-ray reflectometry measurements. We find that the film thickness, t, 3 nm $< t <$ 12 nm, depends linearly on the deposition time. The fine control of the film thickness allowed us to tune the superconducting and normal state properties within the film set, as shown in Figs. 1(b)–1(d).

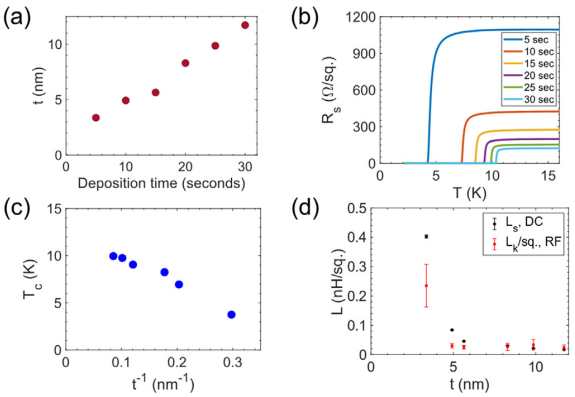

FIG. 1. (a) The thickness (t) of the NbTiN films studied in this work measured by x-ray reflectometry as a function of deposition time. (b) Sheet resistance (R_s) vs temperature (T) indicating a transition from a metallic normal state to the superconducting state at T_c. (c) Superconducting critical temperature (T_c) plotted against the inverse of thickness (t^{-1}). (d) Surface kinetic inductance (L_s), measured by DC transport, and an RF measurement of the kinetic inductance per square ($\frac{L_k}{\text{sq.}}$) as a function of thickness (t), showing an order-of-magnitude increase as a function of decreasing thickness.

To understand the electrical transport properties of these films, we fabricated Hall bars from these films. See the supplementary material for the fabrication details. In Fig. 1(b), we show the sheet resistance (R_s) vs temperature, of each one of the Hall bars in zero applied magnetic field, as measured in a Quantum Design Physical Property Measurement System, down to $T = 2$ K with a DC excitation $\leq 1\ \mu$A. A DC excitation of 1 μA was a sufficiently low current density for all the films such that the superconducting transitions were not broadened. Each film exhibited a superconducting transition upon decreasing the temperature, where we define the superconducting critical temperature (T_c) at zero resistance below a noise level of $\sim 0.2\ \frac{\text{m}\Omega}{\text{sq.}}$. Furthermore, as seen in Fig. 1(c), T_c scales linearly with the inverse of t which has also been observed in superconducting thin films of Nb, Pb, Bi, and MoC.[41–43] This behavior is attributed to the modified Ginzburg–Landau surface boundary conditions of the superconducting order parameter in the thin film geometry.[44]

In Fig. 1(d), we show the surface kinetic inductance (L_s) as a function of t as inferred from the transport properties in Fig. 1(b). For a superconducting slab in the local limit, where $\kappa = \frac{\lambda_{local,0}}{\xi_0} \gg 1$ and $t \ll \lambda_{local,0}$, where $\lambda_{local,0}$ is the local limit penetration depth and ξ_0 is the Ginzburg–Landau coherence length at zero temperature, one can show via Mattis–Bardeen theory that $L_s \approx \frac{\hbar R_s}{\pi \Delta_0}$.[8,11] Here, R_s is the normal state sheet resistance, measured at $T = 15$ K for our films, and $\Delta_0 = 1.764 k_B T_c$. We estimate $\lambda_{local,0}$ from the expression $\lambda_{local,0} \approx 105\ \text{nm} \times \sqrt{\frac{\rho_N}{1\ \mu\Omega-\text{cm}} \frac{1\ \text{K}}{T_c}} = \sqrt{\frac{\hbar \rho_N}{\pi \mu_0 \Delta_0}}$, where ρ_N is the normal state resistivity at $T = 15$ K.[8,11] We find 400 nm $\leq \lambda_{local,0} \leq 1.04\ \mu$m for our films. See the supplementary material for the values. Therefore, $t \ll \lambda_{local,0}$, and thus, our estimate L_s is reasonable. For the $t = 3.36$ nm film, $L_s = 0.403 \pm 0.005\ \frac{\text{nH}}{\text{sq.}}$ and is nearly 24× larger than for the $t = 11.72$ nm film. This is greater than the recently reported value $L_s = 0.115\ \frac{\text{nH}}{\text{sq.}}$ for $Nb_yTi_{1-y}N$ films used for high-kinetic inductance superconducting resonators where the film thickness $t = 5 - 7$ nm.[33]

From each NbTiN superconducting film, we fabricated a set of five $\lambda/4$ coplanar waveguide (CPW) transmission line superconducting resonators capacitively coupled to a central feed line. The other end of the $\lambda/4$ resonator is shorted to a ground plane which surrounds the five resonators and the center feedline CPW. A top-down view of the layout of the resonators is shown in Fig. 2(c) with a measurement schematic. The fabrication details and an enlarged view of the resonator layout are included the supplementary material. Each of the five resonators (R1–R5) was designed with a geometric resonance frequency (f_g) to be in the range of 4–5 GHz and to be capacitively coupled to a center $Z = 50\ \Omega$ feedline CPW. We designed f_g given $f_g = {}^{v_p}/_{4l}$, where $v_p = 0.3956c$ is the phase velocity, c is the speed of light, and l is the length of the resonator, and tuned f_g by varying l.[4] Specifically, we designed R1–R5 to have a decreasing f_g from $f_{g,R1} = 5.18$ GHz to $f_{g,R5} = 4.045$ GHz.

We modeled the characteristic geometric impedance (Z_g) of our resonators using the line calculator option of Quite Universal Circuit

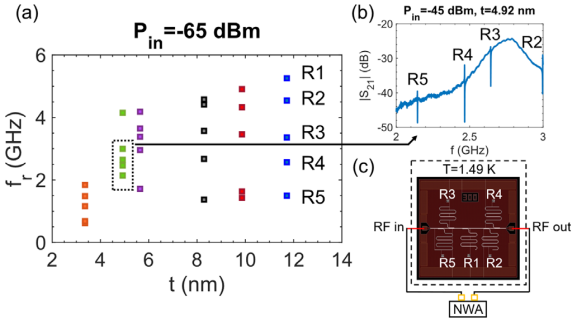

FIG. 2. (a) A plot of each of the five resonant frequencies (f_r) per die (constant color) from resonators R1–R5 at $T = 1.49$ K and RF input power $P_{in} = -65$ dBm. f_r in aggregate increases as function of increasing thickness. (b) Transmission ($|S_{21}|$), in log-magnitude scale, through the coplanar wave guide (CPW) vs frequency (f), showing multiple, well separated resonances between 2 and 3 GHz with $P_{in} = -45$ dBm for the sample with $t = 4.96$ nm. (c) Layout of the resonator die design with five $\lambda/4$ resonators capacitively coupled to a common CPW feedline on a single $6 \times 6\,\text{mm}^2$ die. See the supplementary material for an enlarged view. The HP 8753D network analyzer is denoted as NWA, and P_{in} is measured at the NWA with no added attenuators.

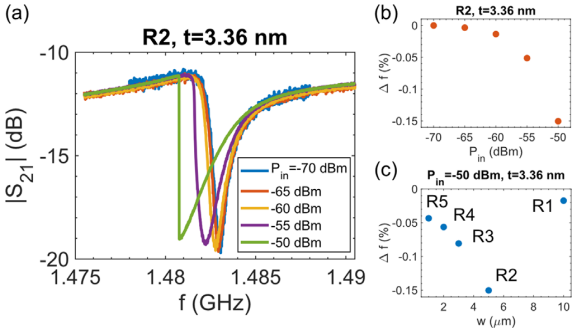

FIG. 3. (a) Frequency-dependent transmission ($|S_{21}|$) at selected RF input powers (P_{in}) in a log-magnitude scale for R2. The discontinuity in the resonance curve at $P_{in} = -50$ dBm indicates a dynamic bifurcation where two metastable resonant oscillation states exist (green trace). (b) Difference in the measured resonant frequency (Δf) with respect to the low power limit in the resonant frequency as a function of P_{in} demonstrating the high kinetic inductance of the superconducting resonator. (c) Δf vs w at $P_{in} = -50$ dBm for the thinnest film.

Simulator (QUCS).[45] Z_g of a transmission line resonator is given by $Z_g = \sqrt{\frac{L_{g,l}}{C_l}}$, where $L_{g,l} = \frac{\mu_0}{4}\frac{K(k_0')}{K(k_0)}$ and $C_l = 4\epsilon_0\epsilon_{eff}\frac{K(k_0)}{K(k_0')}$ are the geometric inductance and capacitance per unit length of the transmission line resonator, $\mu_0 = 4\pi \times 10^{-7}\,\frac{\text{H}}{\text{m}}$, $\epsilon_0 = 8.854 \times 10^{-12}\,\frac{\text{F}}{\text{m}}$, and ϵ_{eff} is the effective dielectric constant of the substrate.[4,46] $K(k)$ is the complete elliptic integral of the first kind with $k_0 = \frac{w}{w+2s}$ and $k_0' = \sqrt{1-k_0^2}$, where w is the width of the center conductor and s is the width of the gap.[4,46] The dimensions and design parameters for R1–R5 are included in the supplementary material. R1 has the widest center conductor width ($w = 10\,\mu$m), while R5 has the narrowest ($w = 1\,\mu$m). At a fixed thickness, the design intention was to have R5 be most sensitive to an applied current.

We measured the transmission through the CPW, S_{21}, as a function of frequency with a HP 8753D network analyzer (NWA) with a measurement bandwidth of 30 kHz–6 GHz. All frequency scans were conducted with a positive frequency sweep direction. All measurements were carried out in a pumped helium closed cycle refrigerator with a base temperature of $T = 1.49$ K, well below T_c of the films, as seen in Fig. 1(c). The RF input power (P_{in}) was measured at the NWA with no added attenuators. At room temperature, the stainless-steel coax lines connecting the top of the refrigerator to the resonator die exhibited 16 dB of loss at 2 GHz and 20 dB of loss at 4 GHz. This provided sufficient thermal isolation at the resonator die at $T = 1.49$ K. Multiple resonances appear as dips in $|S_{21}|$ as seen over a large bandwidth in Fig. 2(b). These resonances are well separated from one another in frequency space and are, thus, easily distinguishable over wideband scans. Over a narrow bandwidth and with decreasing P_{in}, we typically measured a sharp resonance as seen in Fig. 3(a). Taken in aggregate, the resonators have a total quality factor, $1000 < Q < 30\,000$, with Q increasing for decreasing resonator center conductor width. The coupling quality factor, Q_c, controls the width dependence as smaller width resonators have lower f_r and higher Q_c since scales as $Q_c \sim \frac{1}{f_r^2}$ for a transmission line.[47] The internal quality factors, Q_i, in the $t = 3.36$ nm film are $Q_i > 1900$ and are subsequentially larger in the thicker films where $Q_i > 16\,000$ for the $t = 11.72$ nm film.

As seen in Fig. 2(a), we observe a decrease in the measured resonant frequency (f_r) through R1–R5 as a function of decreasing film thickness. Taken in aggregate from Fig. 2(a), there is an overall average decrease in resonant frequency by a factor of ~ 3 between $t = 11.72$ nm and $t = 3.36$ nm. This is simply due to the overall increase in $L_k(0)$ as a function of decreasing thickness, as corroborated in our transport measurements shown in Fig. 1(d). With this in mind, we could easily shrink wavelength dependent dimensions of the resonator, the length l, by a factor of ~ 3, to achieve f_r in the range of $1 - 5$ GHz.

Additionally, the kinetic inductance fraction, defined as $\alpha = \frac{L_k}{L_k + L_g}$, where L_g is the geometric inductance, can be expressed in terms of f_r and f_g. Here, $\alpha = 1 - \left(\frac{f_r}{f_g}\right)^2$ where $f_r = \frac{1}{\sqrt{(L_k+L_g)C}}$, $f_g = \frac{1}{\sqrt{L_g C}}$ and C is the capacitance of the transmission line resonator. For the thinnest film resonator die, $\alpha > 0.87$ for R1–R5. As a function of thickness, R5, for instance, varies from $\alpha = 0.98$ at $t = 3.36$ nm to $\alpha = 0.88$ at $t = 11.72$ nm. Furthermore, given the characteristic impedance of the resonator is $Z_c = \sqrt{\frac{L_{k,l}+L_{g,l}}{C_l}}$, we can express Z_c in terms of α and Z_g, and thus, $Z_c = \frac{Z_g}{\sqrt{1-\alpha}}$. We note that for R5, in the $t = 3.36$ nm film, $\alpha = 0.98$ and $Z_g = 105.4\,\Omega$, therefore $Z_c \approx 750\,\Omega$. The high Z_c is advantageous for spin-photon coupling in quantum dot-superconducting resonator hybrid systems.[32,33]

From α and Z_c, we can extract a $\frac{L_k}{\text{sq.}} = 2\pi\frac{L}{N_{\text{sq}}}$, given the effective inductance and capacitance of the transmission line resonator are $L = \frac{1}{C\omega_r^2}$ and $C = \frac{\pi}{4\omega_r Z_c}$, where $\omega_r = 2\pi f_r$ and $N_{\text{sq.}} = \frac{l}{w}$, the total number of squares comprising the length of the center conductor.[47] For R5, $\frac{L_k}{\text{sq.}} = 0.231 \pm 0.012\,\frac{\text{nH}}{\text{sq.}}$. Averaging $\frac{L_k}{\text{sq.}}$ for R1 through R5 for the $t = 3.36$ nm film, we arrive at $\frac{L_k}{\text{sq.}} = 0.255\,\frac{\text{nH}}{\text{sq.}} \pm 0.09\,\frac{\text{nH}}{\text{sq.}}$. This number is in rough agreement with the L_s for this film, as seen in Fig. 1(d), and

also illustrates that there is a high degree of scatter in the results. In general, because of the high number of squares in the resonator structures, we expect them to be more sensitive to any variations in processing and measurement, especially in the thinnest films.

Although we measured the $t = 3.36$ nm thick film resonators at a finite temperature where $\frac{T}{T_c} \sim 0.4$, the difference between the finite temperature result and the zero-temperature result, for either $\frac{L_k}{\text{sq.}}$ or L_s, was at most a few percent. We can see this by noting the two-fluid expression for $L_k(T)$, where $L_k(T) = \frac{\mu_0 \lambda^2(T) l}{A} \sim \frac{1}{1-(\frac{T}{T_c})^4}$, $\lambda(T)$ is the penetration depth, l is the length of the film, and A the cross-sectional area of the film.[48] For the thinnest film, where $\frac{T}{T_c} \sim 0.4$, $\frac{1}{1-(\frac{T}{T_c})^4} \sim 1.026$, and thus, $\frac{L_k(T)-L_k(0)}{L_k(0)} = 0.026\%$ or 2.6%. Since this difference is small, we ignored thermal effects, due to quasiparticle excitations, in our calculations of $\frac{L_k}{\text{sq.}}$ and L_s.

Furthermore, we demonstrate the nonlinear character of these films through the resonant frequency shift (Δf) vs power (P_{in}), as seen in Fig. 3. The shifts are sufficiently large that parametric amplification is readily achievable. In addition to the shift in f_r as a function of the film thickness, which is simply due to tuning $L_k(0)$, f_r shifts to lower frequencies with increasing P_{in} at a fixed film thickness. This is seen in the second term for the expression for $L_k(I)$, where $\sim L_k(0)\left[(\frac{I}{I_*})^2\right]$ and is most apparent in the thinnest film, as seen in Fig. 3. In Fig. 3(a), for R2, $|S_{21}|$ exhibits a discontinuity in the resonance curve at $P_{in} = -50$ dBm for a frequency sweep from low to high frequency. This discontinuity is indicative of a dynamic bifurcation where two metastable resonant oscillation states exist and is a general characteristic of nonlinear oscillators at large drive amplitudes.[49] Although the value for the dynamic bifurcation power (P_{bif}) depends on the frequency sweep direction, if we were to use R2 as a parametric amplifier, we would pump the resonator near $P_{in} = -50$ dBm at the frequency of the discontinuity in $|S_{21}|$, or in other words, $P_{bif} \approx P_{in} = -50$ dBm.

Although the value for P_{bif} is not unique among the resonators in aggregate, we find that the thinnest film allows for an easily measurable bifurcation at a low P_{in}. For frequency sweeps from low to high frequency, we define Δf as a function of P_{in}, with respect to the low power limit as $\Delta f = 100*(f_r - f_{r,low\,power})/f_{r,low\,power}$, where $f_{r,low\,power}$ is the measured resonant frequency at low power. We use this as a simple measure of the resonator's nonlinearity up to and near P_{bif}. For the five resonators in the thinnest film, Δf ranges from -0.017% to -0.15%, at $P_{in} = -50$ dBm as seen in Fig. 3(c) and is strongest in R2 as seen in Figs. 3(a)–3(c). Upon increasing the film thickness, in our case to $t = 4.92$ nm, Δf at $P_{in} = -50$ dBm is typically reduced an order of magnitude (see the supplementary material).

We further elaborate on the source of the nonlinear RF response of the individual resonators. In general, the nonlinear RF response of the superconductor results from a quasiparticle backflow current density, which depends on the temperature and superfluid velocity.[7] This leads to a current density dependent superfluid density, and thus, a nonlinear kinetic inductance contribution $\sim L_k(0)[(\frac{I}{I_*})^2]$, provided the quasiparticles are in local thermal equilibrium with the condensate.[7] Beyond this picture, spatial variations in the superfluid density as a function of increasing current density, tuned by increasing P_{in} beyond -65 dBm, could lead to a nonequilibrium quasiparticle population in the resonator. For the thinnest film, all the resonators satisfy the condition $t \sim \xi_0 \ll \lambda_{local,0}$. The resonator center conductor widths range from $w_{R5} \sim \lambda_{local,0}$ to $w_{R1} \sim 10\lambda_{local,0}$. Such behavior could manifest itself as an inhomogeneous current flow in the center conductor. However, the strength of the resonators' RF response can vary as seen in Fig. 3(c) at $P_{in} = -50$ dBm and may not only necessarily depend strictly on the macroscopic geometry such as the resonator's width or length but also depend on the microscopic details of the current path.

We finally comment on the properties of these films in terms of the root mean squared roughness (R_q) of the film which we measured by atomic force microscopy (AFM) shown in Fig. 4. Figure 4(a) is a $10 \times 10\ \mu\text{m}^2$ AFM image of a portion of the ground plane in the thinnest film, and Fig. 4(b) is the 3D rendering of the same AFM image to aid visualization. As viewed from either image, the thinnest film is smooth over a large length scale. See the supplementary material for AFM images of the other films. As seen in Fig. 4(c), we measure $R_q = 0.41\ (\pm 0.06)$ nm in the thinnest film as compared to $R_q = 0.77\ (\pm 0.24)$ nm in the thickest film. The thinnest films are continuous, have a larger ρ_N, and thus, have an enhanced $L_k(0)$.

In conclusion, we have measured the resonant frequencies of a collection of high kinetic inductance superconducting $\lambda/4$ NbTiN transmission line resonators as a function of the film thickness in the very thin film and low frequency limit $hf < k_B T$. This enhancement can result in $\Delta f = -0.15\%$ at approximately P_{bif}. The future work will focus on tuning our microfabrication methods to maintain uniformity of the RF response across different resonators on the full $6 \times 6\ \text{mm}^2$ die and design parametric amplifiers from there.

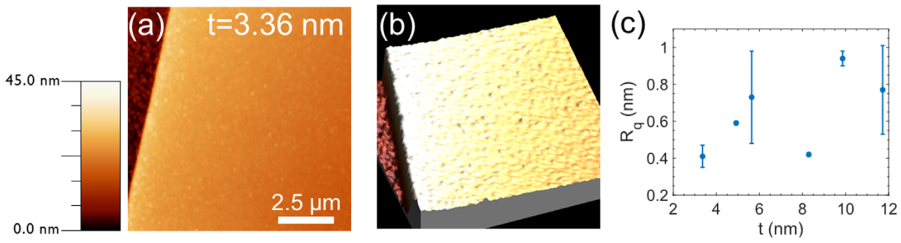

FIG. 4. (a) A $10 \times 10\ \mu\text{m}^2$ AFM image of the ground plane in the thinnest sample with the z-scale on the left. (b) A 3D rendering of the image in (a). (c) The root mean squared roughness (R_q) vs thickness (t) for each film. We note that the thinnest film is continuous as seen in (a) with $R_q = 0.41\ (\pm 0.06)$ nm.

See the supplementary material for additional information on the x-ray reflectivity measurements, Hall bar and resonator fabrication details, design parameters of the resonators, additional RF resonator measurements, and AFM images of the NbTiN thin films.

We thank Eric A. Shaner for the use of his 1K-pot cryostat, Michael C. Wanke for the use of his wirebonder, and William Kindel and Peter A. Sharma for their critical reading of the manuscript. We gratefully acknowledge Sergei Ivanov and Sadhvikas Addamane for their guidance in x-ray reflectometry.

This work was funded by the Laboratory Directed Research and Development Program at Sandia National Laboratories (SNL). SNL is a multimission laboratory managed and operated by the National Technology & Engineering Solutions of Sandia, LLC, a wholly owned subsidiary of Honeywell International Inc., for the U.S. Department of Energy's National Nuclear Security Administration under Contract No. DE-NA0003525. This work was performed, in part, at the Center for Integrated Nanotechnologies, a U.S. DOE, Office of BESs, user facility. A portion of this work was supported by the National Science Foundation under Grant No. DMR-1905909 (S.E. and M.V.).

This paper describes objective technical results and analysis. Any subjective views or opinions that might be expressed in the paper do not necessarily represent the views of the U.S. Department of Energy or the United States Government.

AUTHOR DECLARATIONS

Conflict of Interest

The authors have no conflicts to disclose.

Author Contributions

Terence M. Bretz-Sullivan: Formal analysis (lead); Investigation (equal); Writing – original draft (lead); Writing – review and editing (lead). **Rupert M. Lewis:** Formal analysis (equal); Investigation (equal); Writing – original draft (equal); Writing – review and editing (equal). **Ana L. Lima-Sharma:** Investigation (supporting). **David Lidsky:** Investigation (supporting). **Christopher M. Smyth:** Investigation (supporting). **C. Thomas Harris:** Investigation (supporting). **Michael Venuti:** Investigation (supporting). **Serena Eley:** Investigation (supporting). **Tzu-Ming Lu:** Formal analysis (equal); Investigation (equal); Writing – original draft (equal); Writing – review and editing (equal).

DATA AVAILABILITY

The data that support the findings of this study are available from the corresponding author upon reasonable request.

REFERENCES

[1]A. Blais, A. L. Grimsmo, S. M. Girvin, and A. Wallraff, Rev. Mod. Phys. **93**, 025005 (2021).
[2]B. A. Mazin, AIP Conf. Proc. **1185**, 135 (2009).
[3]Z.-L. Xiang, S. Ashhab, J. Q. You, and F. Nori, Rev. Mod. Phys. **85**, 623 (2013).
[4]M. Göppl, A. Fragner, M. Baur, R. Bianchetti, S. Filipp, J. M. Fink, P. J. Leek, G. Puebla, L. Steffen, and A. Wallraff, J. Appl. Phys. **104**, 113904 (2008).
[5]B. Yurke and E. Buks, J. Lightwave Technol. **24**, 5054 (2006).
[6]E. A. Tholén, A. Ergül, E. M. Doherty, F. M. Weber, F. Grégis, and D. B. Haviland, Appl. Phys. Lett. **90**, 253509 (2007).
[7]T. Dahm and D. J. Scalapino, J. Appl. Phys. **81**, 2002 (1997).
[8]T. Cecil, A. Miceli, O. Quaranta, C. Liu, D. Rosenmann, S. McHugh, and B. Mazin, Appl. Phys. Lett. **101**, 032601 (2012).
[9]G. Wang, C. L. Chang, S. Padin, F. Carter, T. Cecil, V. G. Yefremenko, and V. Novosad, J. Low Temp. Phys. **193**, 134–140 (2018).
[10]N. T. Bronn, Y. Liu, J. B. Hertzberg, A. D. Córcoles, A. A. Houck, J. M. Gambetta, and J. M. Chow, Appl. Phys. Lett. **107**, 172601 (2015); N. T. Bronn, E. Magesan, N. A. Masluk, J. M. Chow, J. M. Gambetta, and M. Steffen, IEEE Trans. Appl. Supercond. **25**, 1700410 (2015).
[11]J. Zmuidzinas, Annu. Rev. Condens. Matter Phys. **3**, 169 (2012).
[12]R. P. Erickson, M. R. Vissers, M. Sandberg, S. R. Jefferts, and D. P. Pappas, Phys. Rev. Lett. **113**, 187002 (2014).
[13]L.-M. Svensson, A. Bengtsson, P. Krantz, J. Bylander, V. Shumeiko, and P. Delsing, Phys. Rev. B **96**, 174503 (2017).
[14]A. Megrant, C. Neill, R. Barends, B. Chiaro, Y. Chen, L. Feigl, J. Kelly, E. Lucero, M. Mariantoni, P. J. J. O'Malley, D. Sank, A. Vainsencher, J. Wenner, T. C. White, Y. Yin, J. Zhao, C. J. Palmstrøm, J. M. Martinis, and A. N. Cleland, Appl. Phys. Lett. **100**, 113510 (2012).
[15]B. Chiaro, A. Megrant, A. Dunsworth, Z. Chen, R. Barends, B. Campbell, Y. Chen, A. Fowler, I.-C. Hoi, E. Jeffrey, J. Kelly, J. Mutus, C. Neill, P. J. J. O'Malley, C. Quintana, P. Roushan, D. Sank, A. Vainsencher, J. Wenner, T. C. White, and J. M. Martinis, Supercond. Sci. Technol. **29**, 104006 (2016).
[16]C. M. Quintana, A. Megrant, Z. Chen, A. Dunsworth, B. Chiaro, R. Barends, B. Campbell, Y. Chen, I.-C. Hoi, E. Jeffrey, J. Kelly, J. Y. Mutus, P. J. J. O'Malley, C. Neill, P. Roushan, D. Sank, A. Vainsencher, J. Wenner, T. C. White, A. N. Cleland, and J. M. Martinis, Appl. Phys. Lett. **105**, 062601 (2014).
[17]H. Wang, M. Hofheinz, J. Wenner, M. Ansmann, R. C. Bialczak, M. Lenander, E. Lucero, M. Neeley, A. D. O'Connell, D. Sank, M. Weides, A. N. Cleland, and J. M. Martinis, Appl. Phys. Lett. **95**, 233508 (2009).
[18]J. Goetz, F. Deppe, M. Haeberlein, F. Wulschner, C. W. Zollitsch, S. Meier, M. Fischer, P. Eder, E. Xie, K. G. Fedorov, E. P. Menzel, A. Marx, and R. Gross, J. Appl. Phys. **119**, 015304 (2016).
[19]W. Chen, D. A. Bennett, V. Patel, and J. E. Lukens, Supercond. Sci. Technol. **21**, 075013 (2008).
[20]J. Gao, M. Daal, A. Vayonakis, S. Kumar, J. Zmuidzinas, B. Sadoulet, B. A. Mazin, P. K. Day, and H. G. Leduc, Appl. Phys. Lett. **92**, 152505 (2008).
[21]J. Burnett, L. Faoro, and T. Lindström, Supercond. Sci. Technol. **29**, 044008 (2016).
[22]D. P. Pappas, M. R. Vissers, D. S. Wisbey, J. S. Kline, and J. Gao, IEEE Trans. Appl. Supercond. **21**, 871 (2011).
[23]J. M. Sage, V. Bolkhovsky, W. D. Oliver, B. Turek, and P. B. Welander, J. Appl. Phys. **109**, 063915 (2011).
[24]T. Polakovic, S. Lendinez, J. E. Pearson, A. Hoffmann, V. Yefremenko, C. L. Chang, W. Armstrong, K. Hafidi, G. Karapetrov, and V. Novosad, APL Mater. **6**, 076107 (2018).
[25]A. A. Adamyan, S. E. Kubatkin, and A. V. Danilov, Appl. Phys. Lett. **108**, 172601 (2016).
[26]J. M. Kreikebaum, A. Dove, W. Livingston, E. Kim, and I. Siddiqi, Supercond. Sci. Technol. **29**, 104002 (2016).
[27]M. Sandberg, M. R. Vissers, J. S. Kline, M. Weides, J. Gao, D. S. Wisbey, and D. P. Pappas, Appl. Phys. Lett. **100**, 262605 (2012).
[28]H. M. Iftekhar Jaim, J. A. Aguilar, B. Sarabi, Y. J. Rosen, A. N. Ramanayaka, E. H. Lock, C. J. K. Richardson, and K. D. Osborn, IEEE Trans. Appl. Supercond. **25**, 1100505 (2015).
[29]A. Bruno, G. de Lange, S. Asaad, K. L. van der Enden, N. K. Langford, and L. DiCarlo, Appl. Phys. Lett. **106**, 182601 (2015).
[30]D. J. Thoen, B. G. C. Bos, E. A. F. Haalebos, T. M. Klapwijk, J. J. A. Baselmans, and A. Endo, IEEE Trans. Appl. Supercond. **27**(4), 1 (2017).
[31]R. Barends, H. L. Hortensius, T. Zijlstra, J. J. A. Baselmans, S. J. C. Yates, J. R. Gao, and T. M. Klapwijk, IEEE Trans. Appl. Supercond. **19**, 936 (2009).
[32]N. Samkharadze, A. Bruno, P. Scarlino, G. Zheng, D. P. DiVincenzo, L. DiCarlo, and L. M. K. Vandersypen, Phys. Rev. Appl. **5**, 044004 (2016).
[33]P. Harvey-Collard, G. Zheng, J. Dijkema, N. Samkharadze, A. Sammak, G. Scappucci, and L. M. K. Vandersypen, Phys. Rev. Appl. **14**, 034025 (2020).

[34]D. Hazra, N. Tsavdaris, A. Mukhtarova, M. Jacquemin, F. Blanchet, R. Albert, S. Jebari, A. Grimm, A. Konar, E. Blanquet, F. Mercier, C. Chapelier, and M. Hofheinz, Phys. Rev. B **97**, 144518 (2018).
[35]E. F. C. Driessen, P. C. J. J. Coumou, R. R. Tromp, P. J. de Visser, and T. M. Klapwijk, Phys. Rev. Lett. **109**, 107003 (2012).
[36]A. Y. Mironov, D. M. Silevitch, T. Proslier, S. V. Postolova, M. V. Burdastyh, A. K. Gutakovskii, T. F. Rosenbaum, V. V. Vinokur, and T. I. Baturina, Sci. Rep. **8**, 4082 (2018).
[37]A. G. Moshe, E. Farber, and G. Deutscher, Appl. Phys. Lett. **117**, 062601 (2020).
[38]M. J. Feldman, P. T. Parrish, and R. Y. Chiao, J. Appl. Phys. **46**, 4031 (1975).
[39]S. Wahlsten, S. Rudner, and T. Claeson, J. Appl. Phys. **49**, 4248 (1978).
[40]M. A. Castellanos-Beltran and K. W. Lehnert, Appl. Phys. Lett. **91**, 083509 (2007).
[41]S. A. Wolf, J. J. Kennedy, and M. Nisenoff, J. Vac. Sci. Technol. **13**, 145 (1976).
[42]M. Strongin, R. S. Thompson, O. F. Kammerer, and J. E. Crow, Phys. Rev. B **1**, 1078 (1970).
[43]S. J. Lee and J. B. Ketterson, Phys. Rev. Lett. **64**, 3078 (1990).
[44]J. Simonin, Phys. Rev. B **33**, 7830(R) (1986).
[45]See http://qucs.sourceforge.net/ for information about QUCS.
[46]C. P. Wen, IEEE Trans. Microwave Theory Tech. **17**, 1087–1090 (1969).
[47]D. M. Pozar, *Microwave Engineering*, 2nd ed. (John Wiley & Sons, Inc., 1998).
[48]M. Tinkham, *Introduction to Superconductivity*, 2nd ed. (Dover, 2004).
[49]F. C. Moon, *Chaotic and Fractal Dynamics* (John Wiley & Sons, Inc., 1992).